2C.6 **EVOLUTION OF AEWs AND MCSs OFF WEST AFRICA OBSERVED DURING AMMA SOP-3 IN SEPTEMBER 2006**

Joël. Arnault[1 *] and Frank. Roux[1]

[1]Laboratoire d'Aérologie (Université de Toulouse and CNRS), Toulouse, France

## 1. INTRODUCTION

Tropical cyclogenesis occurring over the Atlantic off the West African coast during late summer is believed to be driven by scale interaction processes involving the African easterly waves (AEWs), the African easterly jet (AEJ), the south-westerly monsoon flow, the Saharan dry air and the westward propagating mesoscale convective systems (MCSs). It is already known that some Atlantic tropical cyclones have their origin in MCSs propagating over the African continent (Thorncroft and Hodges 2001). For example, Hill and Lin (2003) related the genesis of Hurricane Alberto (2000) to a MCS initiated over the Ethiopian highlands. Lin et al. (2005) documented this case-study and identified three successive convective genesis and lysis periods before the final cyclogenesis event off the Guinea coast. Berry and Thorncroft (2005) also showed that the MCSs associated with the pre-Alberto disturbance were embedded in an AEW. Scale interactions between the MCSs and this AEW certainly contributed to the cyclogenetic evolution of the pre-Alberto disturbance, although the processes involved are not understood yet. This problem can be further investigated by considering more case-studies of developing and non developing West African disturbances.

Here we propose the case of the so-called "Perturbation D" which is a non-developing West African disturbance observed during the Special Observing Period 3 (SOP-3) of AMMA (African Monsoon Multidisciplinary Analysis) that was conducted from Dakar (Senegal) on 15–29 September 2006. This "Perturbation D" was associated with an AEW. Scale interactions between synoptic and convective processes are investigated on the basis of ECMWF (European Center for Mean Weather Forecast) Operational Analyses and brightness temperatures images from Meteosat-9 water vapour channel n°6 (6.85 – 7.85 µm). A Mesoscale simulation has then been conducted with the French non-hydrostatic model Meso-NH. It has been used to compute the energy conversion terms and net advections in the area of this "Perturbation D" to quantify the growth of the wave associated with the disturbance.

* *Corrresponding author address:* Joël Arnault, Laboratoire d'Aérologie, 14 avenue Edouard Belin, 31500 Toulouse, France; e-mail : joel.arnault@yahoo.fr

## 2. DATA

The synoptic environment of the "Perturbation D" is deduced from the ECMWF analyses. Air temperature, relative humidity, geopotential, wind components, relative vertical vorticity and horizontal divergence are available on a regular latitude-longitude grid of resolution 0.5°, at 21 pressure levels between 1000 and 1 mb, at 00 06 12 and 18 UTC.

The convective activity associated with "Perturbation D" is deduced from the Meteosat-9 brightness temperature images in the water vapour channel available every 15 minutes. The Meteosat-9 raw images have been interpolated on a regular latitude-longitude grid of 0.027° resolution and a brightness temperature resolution of 0.5K.

## 3. SIGNATURE OF WAVE ACTIVITY

AEWs have a maximal intensity south of 15°N at the AEJ level at 600-700 hPa (e.g. Carlson 1969a,b; Burpee 1972). Fig. 1a shows a Hovmöller space-time diagram of the ECMWF-analysed relative vertical vorticity at 700 hPa averaged between 5° and 15°N from 22 to 30 September 2006. The tilted black ellipse shows that "Perturbation D" was associated with a well-defined AEW that started on the 22nd afternoon over Ghana (≈0° longitude) and dissipated on the 28th afternoon near the Cape Verde islands (≈25° W). "Perturbation D" also has a distinct signature in the Meteosat-9 images (Fig. 1b) which let suppose interactions between the synoptic wave and the embedded convective activity.

## 4. SCALE INTERACTIONS

Two types of composite images from ECMWF synoptic fields and Meteosat-9 brightness

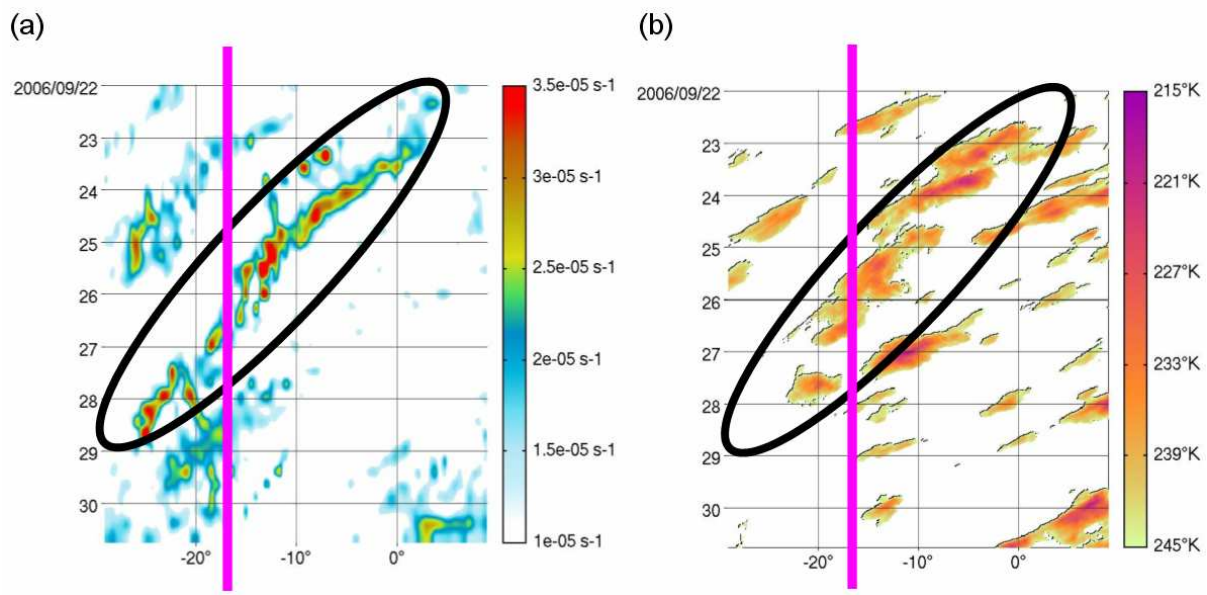


***Figure 1 :*** *(a) Hovmöller space-time diagram of 700 hPa relative vertical vorticity averaged between 5° and 15°N (from ECMWF analyses, colored above +10 $^{5}$ $s^{-1}$) between 22 and 30 september 2006. The X axis indicates longitude in degrees and the Y axis gives time in days. (b) As in (a) except for Meteosat-9 brightness temperature (colored below 245K). In these two diagrams the purple vertical line indicates the mean position of the West African coast and the tilted black ellipse encloses the "Perturbation D".*

temperatures have been used to study scale interaction processes involved in the evolution of "Perturbation D". The first type of composite images (Fig. 2) shows several horizontal fields : brightness temperatures below -30°C indicate convective activity ; the synoptic environment is characterized at 925 hPa by Saharan dry air from north and monsoon surges from south, and at 700 hPa by easterly wind associated with the AEJ and the AEWs. The trough axes of the AEWs have been computed with the objective method proposed by Berry et al. (2006). The whole set of composite images for the "Perturbation D" on 22-28 September 2006 is too voluminous to be included in this paper and only the period from 25 September 2006 at 06 UTC to 27 September 2006 at 18 UTC when the disturbance crosses the West African coast is shown.

The following evolution of "Perturbation D" was deduced from the whole series of composite images. On the 22$^{nd}$ afternoon, the monsoon flow was well established over Ghana and dry Saharan air remained well to the north. The conditions were therefore favourable for convective developments and the growing MCSs have been carried along by the AEJ to south Mali on the 23$^{rd}$. Monsoon surges bringing moist air to "Perturbation D" continued during the two following days. The sustained convective activity strengthened cyclonic curvature of the AEW it was embedded in. On the 25$^{th}$ at 18 UTC (Fig. 2b), "Perturbation D" was over southern Senegal and dry Saharan northerly flow coming from northern Mali enhanced the anti-cyclonic curvature of the AEW. This process intensified during the following days with a dry northerly flow extending westward to Mauritania. Consequently the southerly component of the AEJ related to the anti-cyclonic curvature of the AEW moved "Perturbation D" northward, away from the monsoon flow. During the afternoon of the 27$^{th}$ (Fig. 2f), a last MCS developed off the Senegal coast. It dissipated during the next day as it interacted with a subtropical trough located near the Canary islands.

The second kind of composite image focuses more specifically on the interaction between the synoptic wave and the convective activity (Fig. 3). "Perturbation D" can be associated distinctly with a cyclonic maximum of relative vertical vorticity at 700 hPa, or with the trough of the AEW it is embedded in. Fig. 4 displays the evolution of the vertical profile of relative vertical vorticity averaged over the 6°x6° domain enclosing "Perturbation D" (pink squares in Fig. 3). The associated evolution of the cloud area below different temperature thresholds is also shown in Fig. 4. Following Mathon and Laurent (2000) who used brightness temperature thresholds of -60°C, -40°C, -20°C to describe MCS activity in the Sahel region, convection has been quantified here by the evolution of cloudy surfaces with temperatures colder than -70°C, -50°C and -30°C. Areas colder than -30°C give

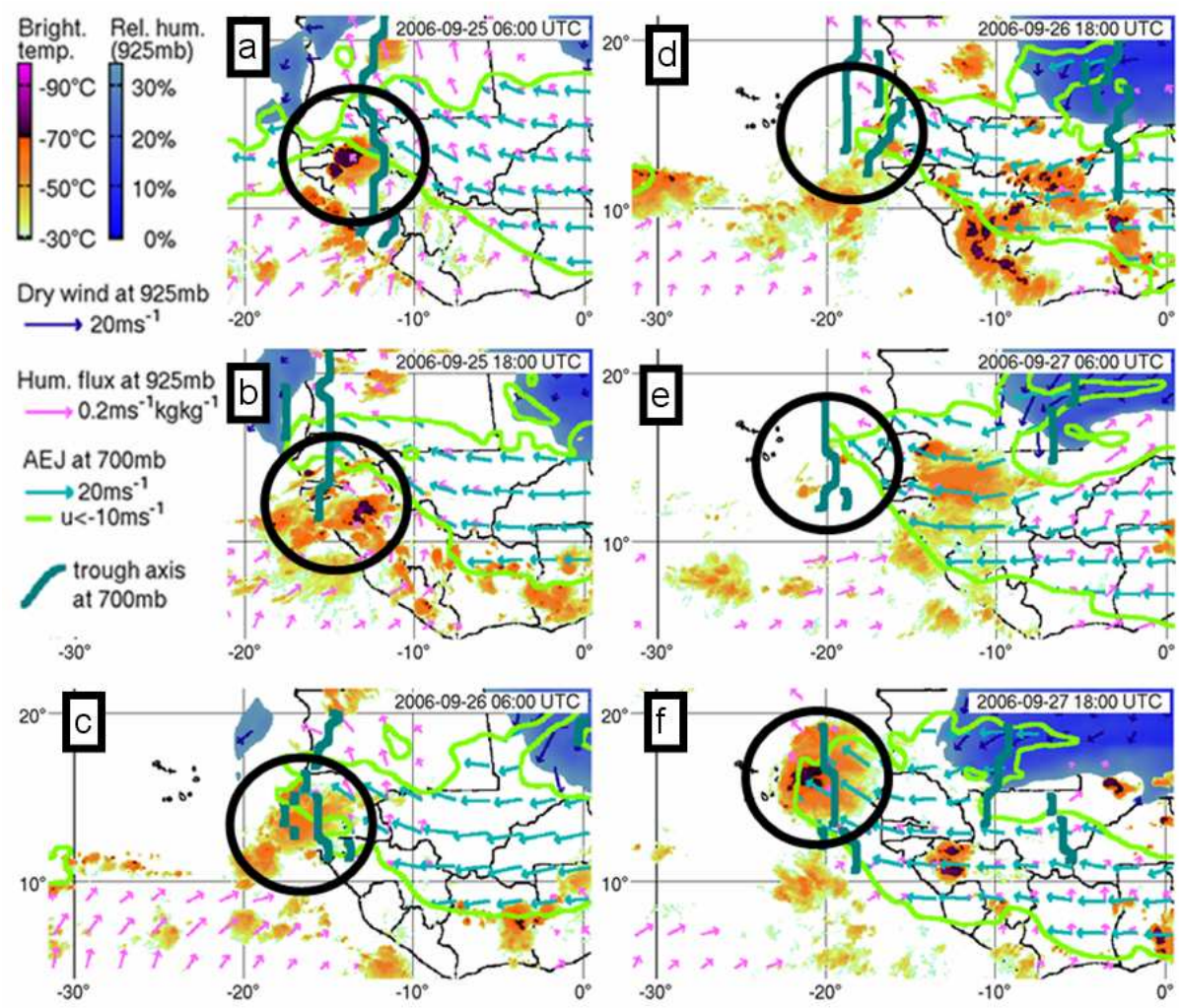


***Figure 2 :*** *Composite images from Meteosat-9 and ECMWF data from (a) 25 September 2006 at 06 UTC till (f) 27 September 2006 at 18 UTC : orange red and black zones show brightness temperature below -30°C, blue areas display relative humidity values less than 30% and northerly wind at 925 hPa, pink arrows represent southerly humidity flux at 925 hPa, bright green lines and blue-green arrows reveal the zonal wind stronger than 10ms$^{-1}$ at 700 hPa, the dark-green lines are the trough axes at 700 hPa computed with the objective method proposed by Berry et al. (2006). The black circles indicate the location of the MCSs associated with "Perturbation D"*

the disturbance's life cycle. The evolution of the area colder than -50°C focuses on convective activity and the evolution of the area colder than -70°C is an indicator of phases of intense convection. Using the pink curve of Fig. 4, three successive stages have been identified for the evolution of "Perturbation D": I : development and propagation over the continent (22-24 September), II : convective re-developments during the crossing of Futa Jallon mountains near the Guinea coast (25-26 September), III : decay over the ocean (27-29 September). The onset of the disturbance and stage I started with surges of intense convection on the evening of 22 and during the 23 September (see black ellipse A in Fig. 4). This was followed by an enhancement of the relative vertical vorticity in the middle atmosphere (see black ellipse B in Fig. 4) which indicates that the growth of the synoptic wave was influenced by convective processes. The deep convective surges actually dissipated on 24 September, but the vorticity disturbance remained visible during the next five days. Stage II is related to the crossing of the mountainous coastal area of Futa Jallon near the Guinea coast. One weak convective re-development occurred over the Futa Jallon mountains on the 25$^{th}$ morning, followed by a convective burst over the ocean in the afternoon, which quickly dissipated on the 26$^{th}$ (see black ellipse C in Fig. 4 and Fig. 2a, b and c). These convective events were also accompanied with an intensification of the cyclonic vorticity around 700-hPa (see black

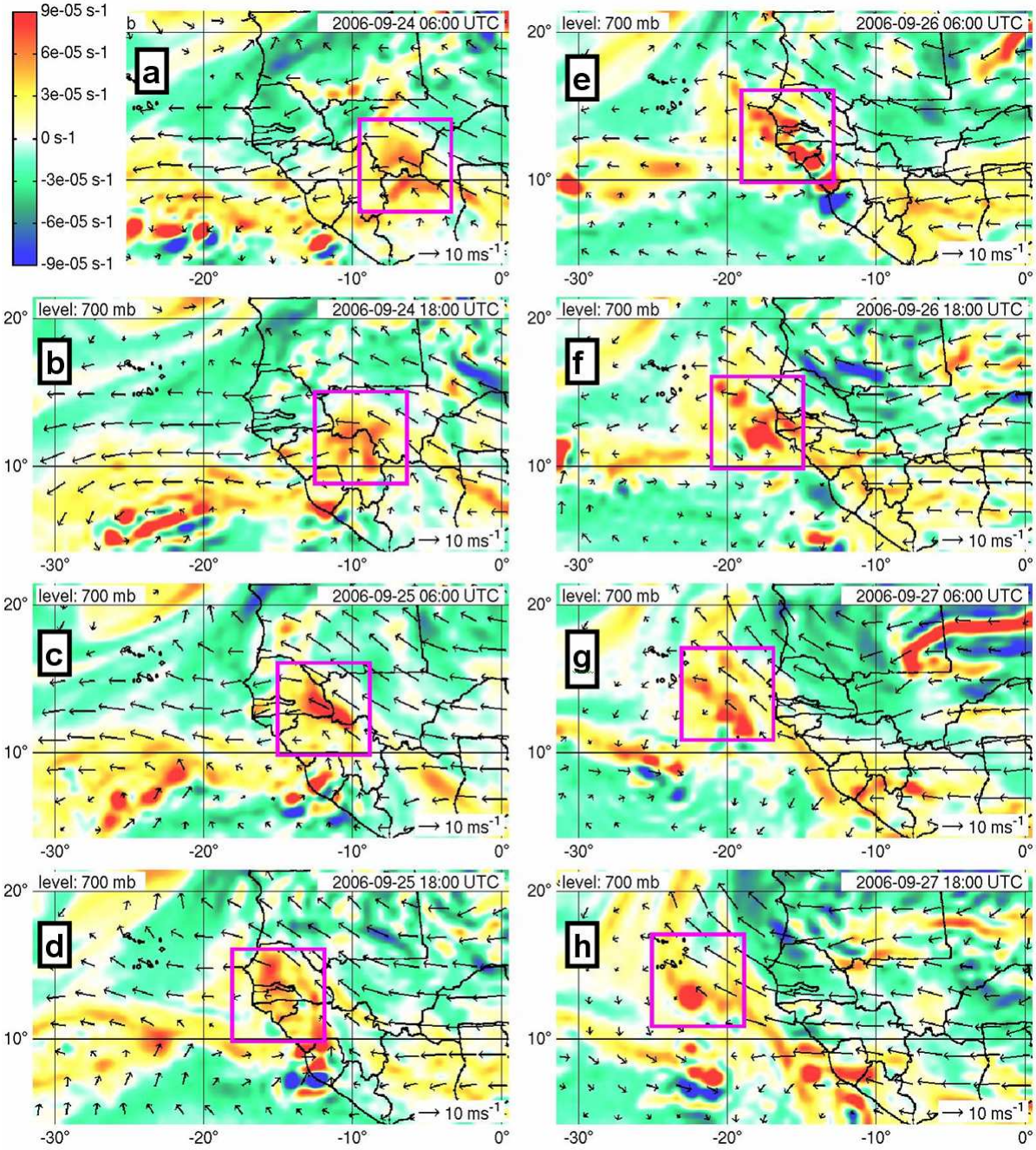


***Figure 3 :*** *Horizontal cross-sections of relative vertical vorticity at 700 hPa derived from the ECMWF analyses for the period from (a) 25 September 2006 at 06 UTC till (h) 27 September at 18 UTC. The 6°x6° pink squares represent the domain wh ere average values have been calculated to characterize "Perturbation D".*

ellipse D in Fig. 4). "Perturbation D" was dissipating in the beginning of the Stage III when a last MCS rapidly grew up off the Senegal coast on the afternoon of 27th (see black ellipse E in Fig. 4 and Fig. 2f), which probably helped to maintain a mid-tropospheric vorticity maximum (see black ellipse F in Fig. 4).

These two composite analyses help to understand the synoptic and convective processes involved in the evolution of "Perturbation D". Monsoon surges over West Africa lead to the formation of MCSs with several genesis and decay phases. These relatively short-lived systems generated cyclonic vorticity anomalies in the middle atmosphere which combined at synoptic level in the AEW. This long-lived vorticity disturbance may then have helped to trigger convective re-developments over the Futa Jallon mountains and over the ocean between the West African coast and the Cape Verde Islands. Such oceanic convective re-development sometimes

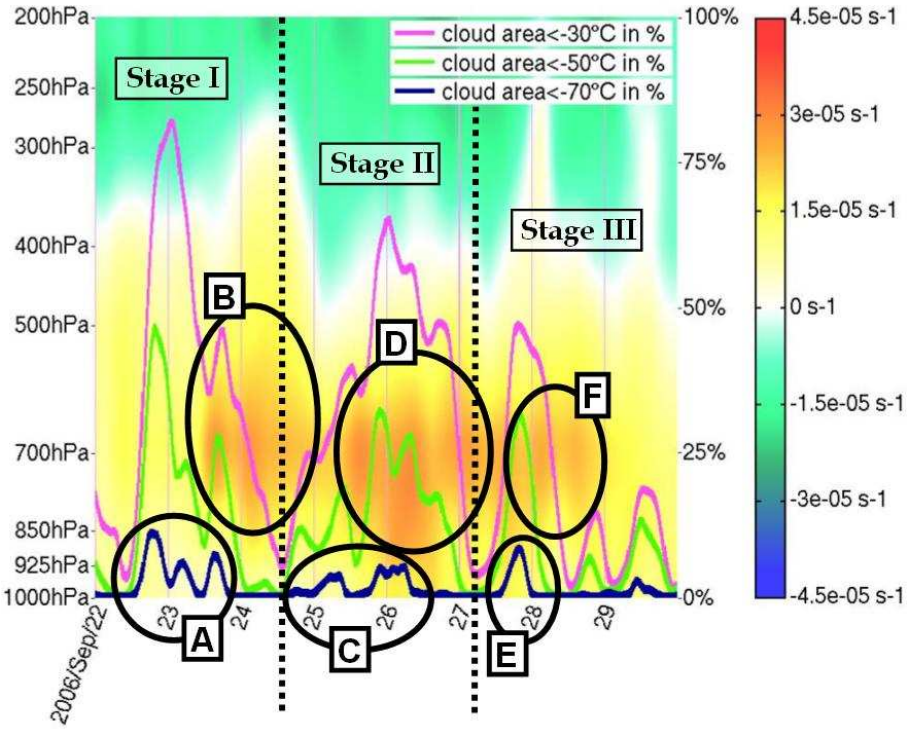


***Figure 4 :*** *Composite image from Meteosat-9 and ECMWF data showing the evolution of several quantities computed in the 6°x6° domain of "Perturb ation D" (see pink squares in Fig. 3) between pressure levels 200 and 1000 hPa. The color contours represent the evolution of the vertical profiles of relative vertical vorticity. The pink, green and blue lines denote the evolution of cloud areas colder than -30°C, -50°C a nd -70°C, respectively. The X axis gives the time in days for the period 22-29 September 2006. The left Y axis corresponds to the pressure levels of the vertical profiles of vertical vorticity, the right Y axis indicates the percentage of the cloudy area in the 6°x6° domain. The colored bar in the right side gives the scale for the relative vertical vorticity. The two vertical dashed black lines delineate the three stages of the "Perturbation D" and the six black ellipses A, B, C, D, E and F enclose features which are discussed in the text.*

leads to a cyclogenesis event although this was not the case for "Perturbation D". In this case indeed, the dry Saharan air coming from northeast during Stage II and III enhanced the anti-cyclonic curvature of the wave, which moved "Perturbation D" northward. Therefore the oceanic convective re-development observed during Stage III was disconnected from the south-westerly monsoon flow, and no cyclogenesis could happen.

It must be outlined that the ECMWF and Meteosat-9 data used for these composite analyses do not simultaneously resolve the synoptic and convective processes. In consequence the scale interactions between the MCSs and the AEW cannot be studied precisely with the composite analyses presented in this section. Mesoscale numerical modelling is needed to obtain a more precise view of the processes involved in "Perturbation D".

## 5. MESOSCALE MODELLING

The French non-hydrostatic mesoscale model Meso-NH has been used to simulate the evolution of "Perturbation D" at high temporal and spatial resolutions and, eventually, to resolve the interactions between the AEW and the MCSs. The simulation presented here has been conducted with two nested models of horizontal resolution 32 and 8 km for the period 24-29 September 2006. The outer domain (model 1) has 160 x 160 points and the inner model 2 has 432 x 240 points. The large scale model is coupled with ECMWF operational analyses at 00, 06, 12 and 18 UTC. The model outputs have been saved every hour. Convective parameterization has been activated for both models so that the scale interactions might not be fully resolved by this numerical approach. It is however expected that the relatively high resolution of model 2 can provide more precise results. A third model with a

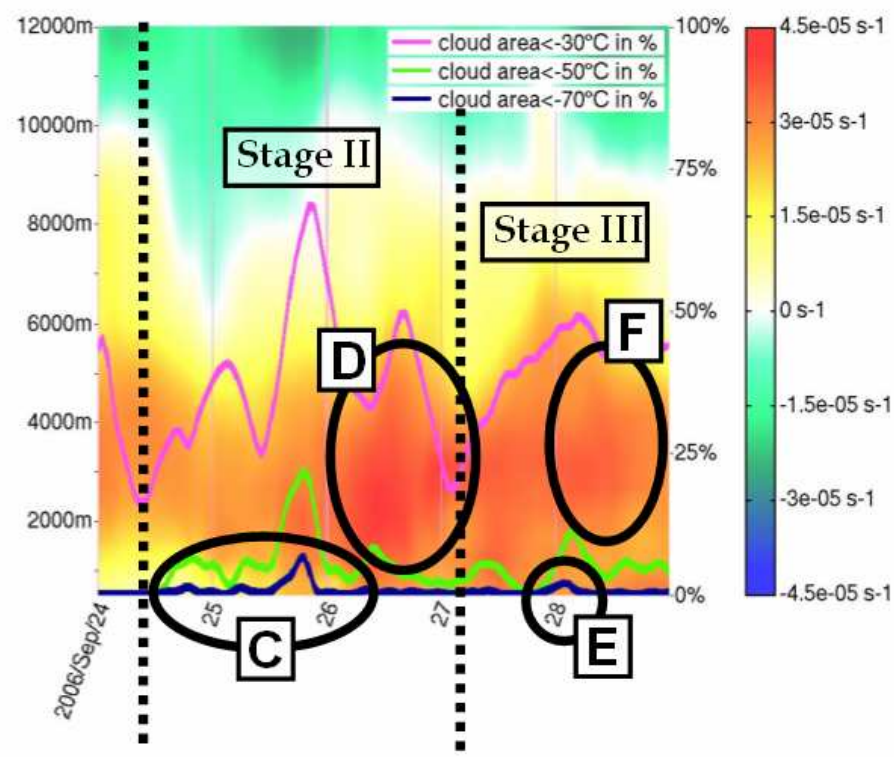


***Figure 5 :*** *As in Fig. 4 except for Meso-NH model 2. The vertical dashed black line delineates the previously defined stages 2 and 3 of "Perturbation D", and the four black ellipses C, D, E and F enclose features which are discussed in the text.*

2km resolution and explicit convection will be activated in a future work.

To evaluate the reliability of the numerical simulation, a composite analysis similar to that discussed in section 4 (Fig. 4) has been applied to the fields produced by Meso-NH model 2 (Fig. 5). The brightness temperature in the Meteosat-9 water vapour channel n°6 were calculated from the Meso-NH results using the RTTOV (Radiative Transfer for Tiros Operational Vertical Sounder) code - version 8.7 (Chaboureau *et al.* 2000). As this Meso-NH simulation starts on 24 September 2006 at 00 UTC, the series of initial convective surges and the resulting vorticity enhancement on 23 and 24 September displayed in Fig 4 (see black ellipses A and B in Fig. 4) do not appear in Fig 5. Nevertheless, the simulated area colder than -30°C (pink curve in Fig. 5) allows to identify stages II and III of "Perturbation D" relatively similar to those in Fig. 4. In particular, Meso-NH simulates a deep convective event on the 25$^{th}$ afternoon (see black ellipse C of Fig. 5) which was observed in Meteosat-9 images a few hours later (see black ellipse C of Fig. 4). This convective event is then followed by an enhancement of vorticity in the mid-troposphere (see black ellipse D of Fig. 5). The last convective event on the 27$^{th}$ afternoon (see the black ellipse E of Fig. 4) has been caught by the Meso-NH simulation, though a few hours later and with a smaller intensity (see black ellipse E of Fig. 5). We can therefore conclude that the Meso-NH simulation is not in contradiction with the observed evolution.

To study qualitatively the finer scale structure brought by the Meso-NH model 2 at 8 km horizontal resolution, the Ertel potential vorticity (EPV) on the 315 K isentrope level, where the AEWs have their maximal activity, is displayed. Berry and Thorncroft (2005) also used this quantity to study the pre-Alberto disturbances over the African continent. The accuracy of the EPV to study the scale interaction between convection and the synoptic processes relies on the hypothesis that the synoptic circulation associated with this "Perturbation D" verifies the thermal wind balance. In that case this synoptic circulation depends only on the EPV and boundary conditions. As EPV is a conservative quantity for adiabatic processes, it is created by latent heating associated with convective systems and is consequently a convective tracer at synoptic scale. The fact that the synoptic circulation associated with "Perturbation D" verifies the thermal wind balance is however questionable at such low latitude and we will investigate this point in details in a future work.

EPV fields at 315 K from ECMWF data and from Meso-NH model 2 are shown in Fig. 6. Whereas the EPV signature of "Perturbation D"

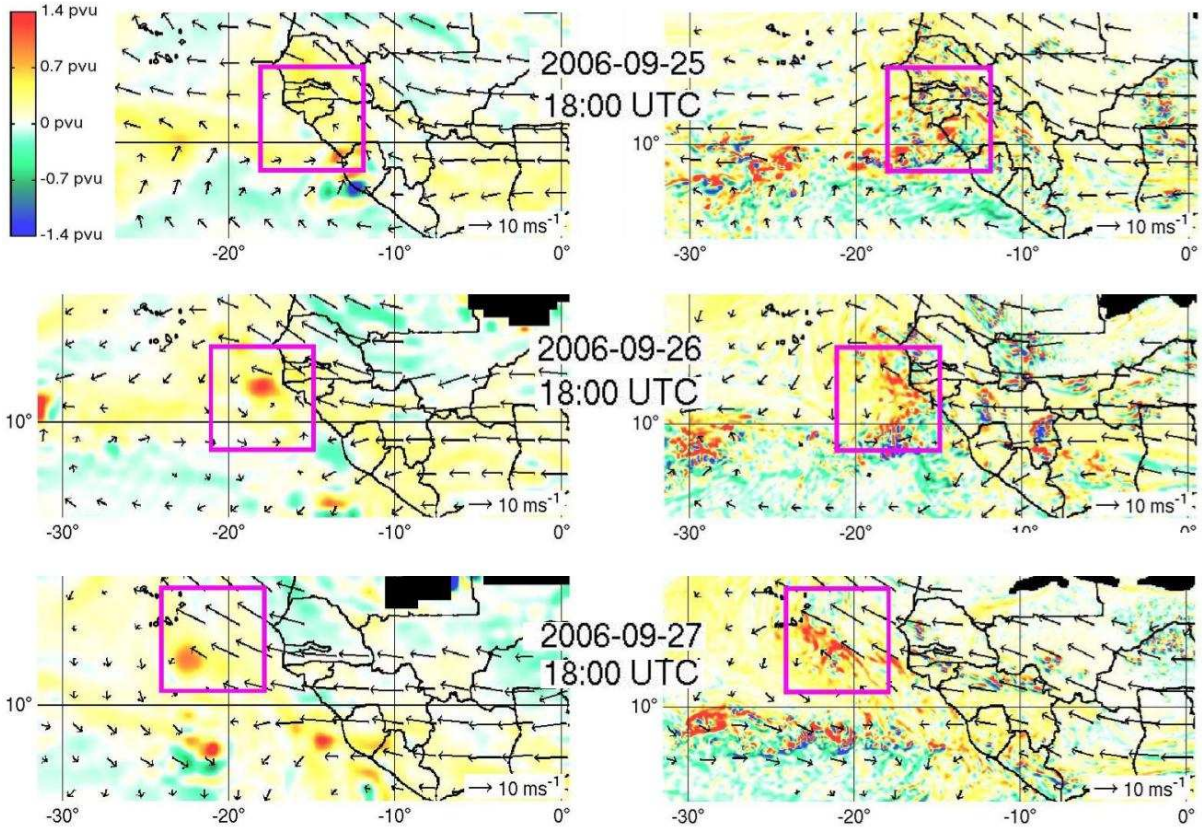


***Figure 6 :*** *Horizontal cross sections of Ertel potential vorticity on the isentropic level 315 K from 25 September 2006 at 18 UTC till 27 September 2006 at 18 UTC. The images in the left column are from ECMWF fields, those on the right are from the Meso-NH model 2. The 6°x6° pink squares represent the domain of "Perturb ation D" previously defined.*

in ECMWF data is only a single maximum, Meso-NH model 2 reveals finer scale structures of convective origin. These small vortices are preferentially created during the late afternoon in connexion with the diurnal cycle of convection. This process was particularly intense on the 25th at 18 UTC when "Perturbation D" was over the Futa Jallon mountains. These convective and orographically induced small scale vortices partly merged over the ocean, then strengthened the disturbance. These results at higher resolution confirm the role of convection in the growth of the wave although modelling with explicit convection is needed for a more quantitative study.

## 6. GROWTH OF THE WAVE

The AEW associated with the "Perturbation D" is a synoptic process which seems to be partly controlled by convection. In order to complete the qualitative analyses of section 4 and 5, the growth of the wave is investigated with the model 2 of Meso-NH. The role of convection in the growth of the synoptic wave will however be approximately estimated as this Meso-NH simulation still used parameterized convection. The energy of the AEW is defined as the eddy kinetic energy ($K_{eddy}$) computed in the 6°x6° domain enclosing the disturbance (see pink squares in Fig. 3) between the altitudes 1000 and 18000 m. There are then four possible sources of energy to explain the growth or decay of this wave energy: zonal kinetic energy ($K_{zonal}$), zonal available potential energy ($A_{zonal}$), eddy available potential energy ($A_{eddy}$) and energy released by latent heating in convection. These energies are also computed in the 6°x6° domain enclosing the disturbance between the altitudes 1000 and 18000 m. Conversion of $K_{zonal}$ to $K_{eddy}$ is the "barotropic" mechanism. Conversion of $A_{zonal}$ to $A_{eddy}$ followed by conversion of $A_{eddy}$ to $K_{eddy}$ is the "baroclinic" mechanism. It has been hypothesized in the previous section that convection played a significant role in enhancing the wave disturbance, although barotropic and baroclinic mechanisms might also have a non-negligible contribution. The growth of wave energy is usually investigated with the system of equations originally proposed by Lorenz (1955), and firstly applied to AEWs by Norquist et al. (1977). The four energy conversion rates ($K_{zonal} \rightarrow K_{eddy}$ ; $A_{zonal} \rightarrow A_{eddy}$ ; $A_{eddy} \rightarrow K_{eddy}$ ; eddy

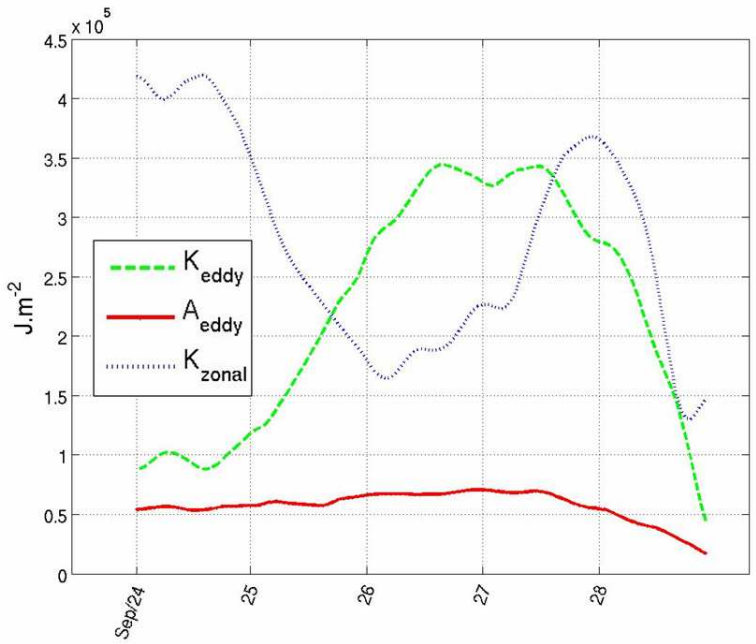


***Figure 7 :*** *Time evolution for the period 24-29 September 2006 of $K_{eddy}$ (green dashed line), $A_{eddy}$ (red line) and $K_{zonal}$ (blue dotted line) computed from the Meso-NH model 2 in the 6°x6° domain enclosing the "Perturbation D" between the altitudes 1000 to 18000 km. The X axis refers to the time in days and the Y axis gives the energy in $Jm^{-2}$. These curves have been obtained after having equilibrated the energetic budget.*

diabatic energy source→$A_{eddy}$) are computed in the 6°x6° domain enclosing "Perturbation D" between the altitudes 1000 and 18000m. The analytic expressions of these rates can be found in Muench (1965) and Norquist et al. (1977). In this particular case it has to be noted that the energy of the wave can also come from outside the considered domain, which is why we also computed the net advection terms of $K_{zonal}$, $K_{eddy}$ $A_{eddy}$ and $A_{zonal}$.

In order to have consistent results the energetic budget has been equilibrated. This operation did not change the general shape of the different curves although the energy variations are somewhat changed. We therefore only discuss the main features of this budget. The time evolutions of the equilibrated energies associated with "Perturbation D" are given in Fig. 7. The equilibrated conversion rates and net advection terms are then provided at Fig. 8. The net advection of $A_{zonal}$ is not represented as the contribution of $A_{zonal}$ to the wave energetic budget is negligible.

The green dashed curve of Fig. 7 shows the evolution of $K_{eddy}$ for the period 24-29 September 2006. It is remarkable that $K_{eddy}$ increased by approximately a factor of four (from 1 $x10^5$ to 3.5 $x10^5$ $Jm^{-2}$) during the 25 and 26 September, which is coherent with the cyclonic vorticity intensification at 700-hPa on the 26, indicated by the black ellipse D of Fig. 5. The wave energy remained high until the 27$^{th}$ afternoon when the last convective burst of 'Perturbation D" occurred. The fast decrease of $K_{eddy}$ from the 28$^{th}$ morning is in agreement with the dissipation of the disturbance.

The most striking feature in Fig. 8 is the positive correlation between the $K_{eddy}$ production by $A_{eddy}$ (dashed green line in Fig. 8) and the $A_{eddy}$ production by the eddy diabatic source of energy (dashed red line in Fig. 8) during all the simulation period, and especially during the 25 and 26 September when the system crosses the Futa Jallon. The conversion rate of $A_{zonal}$ to $A_{eddy}$ (solid blue line in Fig 8) was negligible as well as the advection of $A_{eddy}$ (dashed magenta line in Fig 8). Moreover the conversion rate of $K_{zonal}$ to $K_{eddy}$ (dotted red line in Fig 8) was too small to be considered significant until the 27 September. Consequently during the 25-26 September the growth of the wave associated with "Perturbation D" was mainly baroclinic and conducted by convection. This increase is reduced by a negative net advection of $K_{eddy}$ although this is the result of the budget equilibration. Let's also notice that $A_{eddy}$ produced by the release of latent heating is directly converted to $K_{eddy}$, which is why $A_{eddy}$ remains small (red solid curve in Fig. 7).

The conversion rate of $K_{zonal}$ to $K_{eddy}$ (dotted red line in Fig. 8) started to be significantly negative from the 27 morning, which means that wave energy was converted to zonal energy by an "inverse barotropic" mechanism. This is why

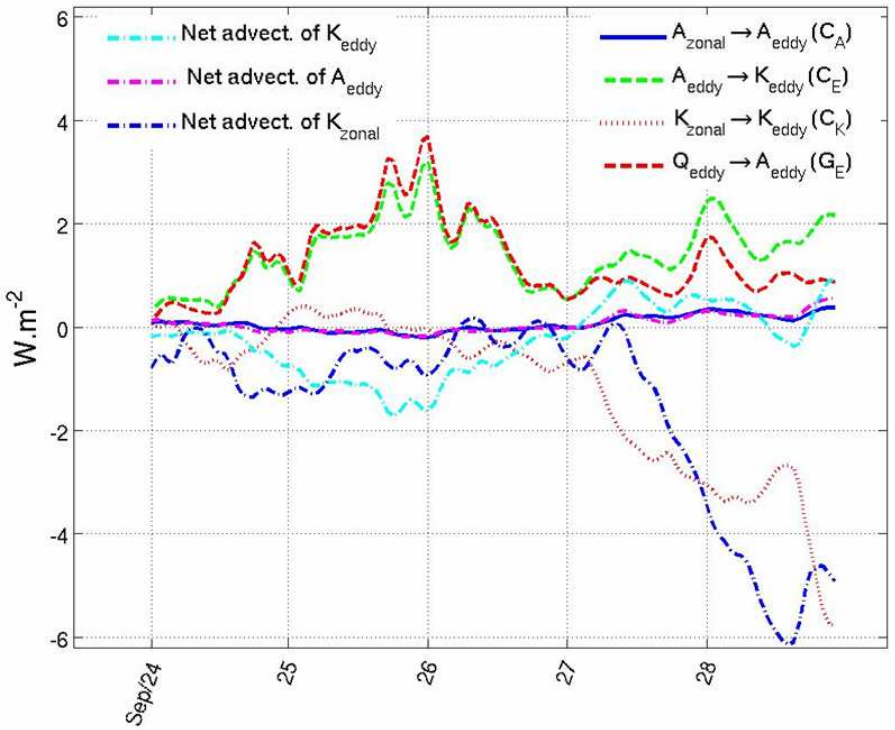


***Figure 8:*** *Time evolution for the period 24-29 September 2006 of the four energy conversion rates ($K_{zonal} \rightarrow K_{eddy}$ ; $A_{zonal} \rightarrow A_{eddy}$ ; $A_{eddy} \rightarrow K_{eddy}$ ; eddy diabatic sources$\rightarrow K_{eddy}$) and of the net advection terms of $K_{eddy}$, $A_{eddy}$ and $K_{zonal}$ computed from the Meso-NH model 2 in the 6°x6° domain enclosing the "Perturbation D" between the altitudes 1000 to 18000 km. The X axis refers to the time in days and the Y axis gives the energy tendencies in Wm$^{-2}$. These curves have been obtained after having equilibrated the energetic budget.*

$K_{zonal}$ grows by a factor of one and a half (from 2.3 x10$^5$ to 3.6 x10$^5$ Jm$^{-2}$) during that day. However the net advection of $K_{zonal}$ decreases dramatically from the 27 afternoon and on the 28 September there is more $K_{zonal}$ advected outside of the disturbance's domain than produced inside by an "inverse barotropic" mechanism. This is why $K_{zonal}$ starts to decrease from that day. This might be interpreted as a complete baroclinic cycle: $A_{eddy}$ produces $K_{eddy}$ which in turn produces $K_{zonal}$.

In conclusion the results from Meso-NH model 2 confirmed the important role played by convection in the growth of the wave associated with "Perturbation D" as it crossed the West African coast near the Futa Jallon. A future work will be to compare this evolution with other case-studies of developing disturbances to see if this interaction usually happens before the off-shore tropical cyclogenesis event.

## 7. PERSPECTIVES

The results derived from Meteosat-9 images, ECMWF analyses and Meso-NH numerical simulations for "Perturbation D" observed during AMMA SOP-3 in September 2006 confirm previous findings on the complex interactions between convection and African Easterly Waves at meso- and synoptic scales (e.g. Berry and Thorncroft 2005). Further information will be obtained on the role played by convection through the analysis of Meso-NH model 3 results at 2 km horizontal resolution. We also compare this situation with those associated with the pre-cyclogenesis phases of Tropical Storm Debby (18-21 August 2006), Hurricane Helene (9-13 September 2006) and Hurricane Dean (8-12 August 2007).

## BIBLIOGRAPHY


Berry, G. and C. Thorncroft, 2005: Case study of an intense African easterly wave, *Mon. Wea. Rev.*, **133**, 752-766

——-—, ——-— and T. Hewson; 2006: African easterly waves during 2004 – analysis using objective techniques, *Mon. Wea. Rev.*, **135**, 1251-1267.

Burpee, R. W., 1972: The origin and structure of easterly waves in the lower troposphere of North Africa, *J. Atmos. Sci.*, **29**, 77-90.

Carlson, T. B., 1969a: Synoptic histories of three African disturbances that developed into

Atlantic hurricanes, *Mon. Wea. Rev.*, **97**, 256-288.

——-—, 1969b: Some remarks on African disturbances and their progress over the tropical Atlantic, *Mon. Wea. Rev.*, **97**, 716-726.

Chaboureau, J.-P., J.-P. Cammas, P. Mascart, J.-P. Pinty, C. Claud, R. Roca, and J.-J. Morcrette, 2000: Evaluation of a cloud life-cycle simulated by Meso-NH during FASTEX using METEOSAT radiances and TOVS-31 cloud retrievals. *Quart. J. Roy. Meteor. Soc.*, **126**, 1735-1750.

Hill, C., M., and Y.-L. Lin, 2003: Initiation of a mesoscale convective complex over the Ethiopian Highlands preceding the genesis of Hurricane Alberto (2000). *Geophys. Res. Lett*, **30**, 1232, doi:10.1029/2002GL016655.

Lin, Y.-L., K. E. Robertson, and C. M. Hill, 2005: Origin and propagation associated with an African easterly wave as a precursor of hurricane Alberto (2000). *Mon. Wea. Rev*., **133**, 3276-3298.

Lorenz, E. N., 1955: Available potential energy and the maintenance of the general circulation. *Tellus*, **7**, 157-167.

Mathon V., and H. Laurent, 2000: Life cycle of sahelian mesoscale convective cloud systems. *Q. J. Meteorol. Soc.*, **127**, 377-406.

Mesinger, F. and A., Arakawa, 1976: Numerical Methods Used in Atmospheric Models. Vol. I, *GARP Publications Series* No. 17, WMO, Geneva, Case Postale No. 2300, CH-1211 Geneve 2, 64 pp

Muench, H. S., 1965: On the dynamic of the wintertime stratospheric circulation, *J. Atmos. Sci.*, **22**, 349-360.

Norquist D. C., E. E. Recker and R. J. Reed, 1977: The energetics of African wave disturbances as observed during phase III of GATE, *Mon. Wea. Rev.*, **105**, 334-342.

Thorncroft, C. D., and K. I. Hodges, 2001: African easterly wave variability and its relationship to Atlantic tropical cyclone activity. *J. Climate*., **14**, 1166-1179.

## ACKNOWLEDGEMENTS

The AMMA SOP-3 field campaign was funded by CNES (French space agency). Pilots and technical crews of the Falcon must be thanked for their cooperation and dedication. Numerical simulations were conducted on CNRS / IDRIS computer under grants 070591 and 080591. We thank Didier Gazen and Juan Escobar for the technical support in Meso-NH, Dr. Jean-Pierre Chaboureau for the scientific support in Meso-NH.